Journal of Scientific & Industrial Research
Vol. 67, June 2008, pp. 412-420

Wavelet-based neural network and statistical approaches applied to automated visual inspection of LED chips

Hong-Dar Lin[1]*, Gary C Lin[2], Chung-Yu Chung[1], and Wan-Ting Lin[3]

[1]Department of Industrial Engineering and Management, Chaoyang University of Technology, 168 Jifong E. Rd., Wufong Township, Taichung County, 41349, Taiwan

[2]Department of Industrial and Manufacturing Engineering and Technology, Bradley University, 1501 West Bradley Avenue, Peoria, IL 61625, USA

[3]College of Business, University of Missouri-Columbia, 213 Cornell Hall, Columbia, MO 65211, USA

Received 17 July 2007; revised 02 April 2008; accepted 04 April 2008

This research explores automated visual inspection of surface defects in a light-emitting diode (LED) chip. One-level Haar wavelet transform is first used to decompose a chip image and extract four wavelet characteristics. Then, wavelet-based back-propagation network (WBPN) and wavelet-based Hotelling statistic (WHS) approaches are respectively applied to integrate multiple wavelet characteristics. Finally, back-propagation algorithm of WBPN or Hotelling test of WHS judges existence of defects. Two proposed methods achieve detection rates of above 90.8% and 92.4%, and false alarm rates below 4.4% and 6.1%, respectively. A valid computer-aided visual defect inspection system is contributed to help meet quality control needs of LED chip manufacturers.

Keywords: Automated visual inspection, Back-propagation network, Hotelling statistic, LED chip production, Wavelet characteristics

Introduction

Automated visual inspection of surface defects has become a critical task for manufacturers who strive to improve product quality and production efficiency[1-3]. With the popularity of light-emitting diodes (LEDs), inspection of surface defects has become a critical task for manufacturers who strive to enhance LED product quality. Automated inspection of a water-drop defect is difficult because the blemish has a semi-opaque appearance and a low intensity contrast with the rough exterior of LED chip. LED chip (width, 0.21mm) comprises an aluminum-pad (bonding pad) in central area and a metal oxide semiconductor (emitting area) in outer area (Fig. 1 a). A water-drop defect may fall across two areas of significantly different textures, which complicates defect detection procedure (Fig. 1 b-d). Defect detection techniques are generally classified into spatial domain and frequency domain. Siew *et al*[4] applied co-occurrence matrix method to assess carpet wear by using two-order gray level statistics to build up probability density functions of intensity changes. For another spatial domain example, Latif-Amet *et al*[5] presented wavelet theory and co-occurrence matrices for detection of defects encountered in textile images and classified each sub-window as defective or non-defective with a Mahalanobis distance.

Chan & Pang[6] proposed a simulated fabric model based on Fourier transform for inspection of structural defects in fabric. Kumar & Pang[7] presented a new multi-channel filtering scheme for unsupervised fabric defect detection using a class of self-similar Gabor functions. Lin & Ho[8] developed an approach that applies discrete cosine transform based enhancement for detection of pinhole defects on passive component chips. Lin & Chiu[9] used multivariate Hotelling T^2 statistic to integrate different coordinates of color models for MURA-type defect detection on liquid crystal displays (LCD), and applied ant colony algorithm and back-propagation neural network (BPNN) techniques to develop an automatic inspection procedure. Lu & Tsai[10] adopted

*Author for correspondence
E-mail: hdlin@cyut.edu.tw

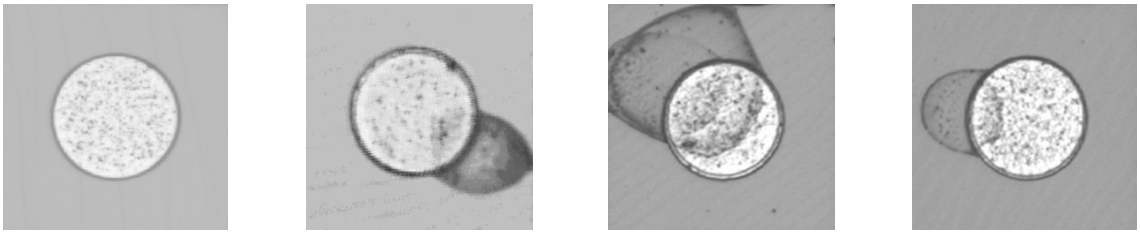

(a) (b) (c) (d)

Fig. 1—LED chip images: a) LED chip without defect; b), c) and d) LED chips with water-drop defects of different shapes

singular value decomposition (SVD) that suits the need for detecting defects on TFT-LCD images of highly periodical textural structures. In recent decade, vision systems have been developed for inspection of surface defects on semiconductor wafers[11-13]. Fadzil & Weng[14] implemented a vision inspection system that achieves a 90% probability of accurately classifying defects, scratches, contamination, blemishes, off center defects, etc. in the encapsulations of diffused LED products.

This study presents an efficient and effective technique that detects semi-opaque and low-intensity-contrast water-drop defects falling across two different background textures.

Proposed Wavelet-based Neural Network and Statistical Method

To detect water-drop defects of LED chips, this study adopts one-level Haar wavelet transform to conduct image transformation and extract wavelet characteristics. Wavelet-based BPNN and multivariate statistical approaches were applied to integrate multiple wavelet characteristics and then develop back-propagation algorithm of neural network model and T^2 test of multivariate statistical analysis to individually judge the existence of water-drop defects in LED chip images.

Wavelet Transform and Properties

Wavelet transform decomposes function V_j in terms of wavelet bases $V_{j-1} \oplus W_{j-1}$. That is, wavelet analysis can deal with the decomposition and synthesis of V_j and V_{j+1} in two-level scaling space. Decomposition conducts a forward wavelet analysis to decompose the base V_{j+1} into bases V_j and W_j. Synthesis performs a backward wavelet analysis to reconstruct V_j and W_j into V_{j+1}[15].

Haar wavelet transform is one of the simplest and basic transformations. Its base transform in multiple-level scaling space can be implemented as

$$v_{j,k} = \frac{v_{j+1,2k} + v_{j+1,2k+1}}{2};\ w_{j,k} = \frac{v_{j+1,2k} - v_{j+1,2k+1}}{2} \quad \ldots (1)$$

In this study, a standard decomposition that covers wavelet row and column transfers to do wavelet transform of a two-dimensional image is applied. Haar transform can be computed stepwise by mean value and half of the differences of tristimulus values of two contiguous pixels. 2-D wavelet transform has been performed by applying 1-D wavelet transform first on rows and then on columns. Based on the transfer concept of one-dimensional space, Haar wavelet transform can process a two-dimensional image of (M x N) pixels in as

Row transfer:

$$\begin{cases} g_R(p,q) = \left[\dfrac{g(p,2q) + g(p,2q+1)}{2} \right], \\ g_R(p, q+\left[\dfrac{N}{2}\right]) = \left[\dfrac{g(p,2q) - g(p,2q+1)}{2} \right], \\ where\ 0 \le p \le (M-1),\ 0 \le q \le \left[\dfrac{N}{2}\right] - 1,\ [\,]\ is\ Gauss\ symbol. \end{cases}$$

Column transfer:

$$\begin{cases} g_C(p,q) = \left[\dfrac{g_R(2p,q) + g_R(2p+1,q)}{2} \right], \\ g_C(p+\left[\dfrac{M}{2}\right], q) = \left[\dfrac{g_R(2p,q) - g_R(2p+1,q)}{2} \right], \\ where\ 0 \le p \le \left[\dfrac{M}{2}\right] - 1,\ 0 \le q \le (N-1). \end{cases} \quad \ldots (2)$$

In above expressions [Eq. (2)], $g(p,q)$ represents an original image, $g_R(p,q)$ the row transfer function of $g(p,q)$, and $g_C(p,q)$ the column transfer function of $g_R(p,q)$. As $g_C(p,q)$ is also the outcome of wavelet decomposition of $g(p,q)$, outcomes of a wavelet transform can be defined as

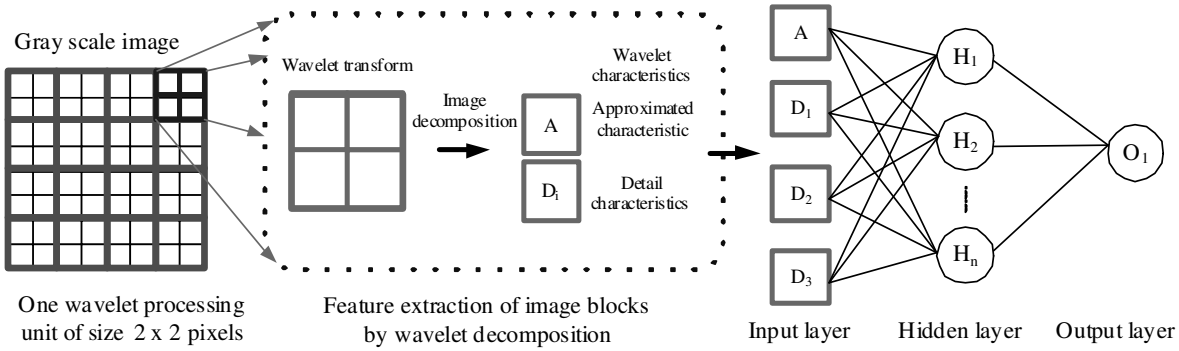

Fig. 2—Network structure of proposed WBPN approach

$$\begin{cases} A(p,q) = g_C(p,q); \quad D_1(p,q) = g_C(p, q+\left[\frac{N}{2}\right]); \\ D_2(p,q) = g_C(p+\left[\frac{M}{2}\right], q); \quad D_3(p,q) = g_C(p+\left[\frac{M}{2}\right], q+\left[\frac{N}{2}\right]); \\ where\ 0 \le p \le \left[\frac{M}{2}\right]-1, 0 \le q \le \left[\frac{N}{2}\right]-1. \end{cases} \quad \ldots(3)$$

One level of wavelet decomposition generates one smooth sub-image (A) and three detail sub-images (D_1, D_2 and D_3) that contain fine structures with horizontal, vertical and diagonal orientations. These four sub-images (size of each image, $M/2$ x $N/2$ pixels) form wavelet characteristics. Wavelet transform provides a convenient way for a multi-resolution representation, from which texture features can be easily extracted. The merits of wavelet transform include local image processing, simple calculations, high speed processing and multiple image information[16,17].

Wavelet-based Back-propagation Network Approach (WBPN)

WBPN approach decomposes an image of (S x T) pixels into a set of sub-images, each of which has a size of (s x t) pixels and is a wavelet processing unit. Original image has u x v (S/s x T/t) wavelet processing units. For each wavelet processing unit, wavelet transform can be applied to the region of (s x t) pixels to obtain four wavelet characteristics (A, D_1, D_2 and D_3) through calculations. This study uses MLP (multi-layer perceptron) neural network with back-propagation algorithm[18-21] to detect defective regions containing water-drop blemishes. Four wavelet characteristics (FWCs) have been used as inputs of neural network model to identify regions with water-drop defects. FWCs describe surface variations of gray level uniformity.

Proposed method (Fig. 2) uses FWCs of a wavelet processing unit as input values of MLP neural network model. If the size of a wavelet processing unit is 2x2 pixels, an image of 256 x 256 pixels will have 16,384 sets of wavelet characteristics. Each set of wavelet characteristics can be judged as in-control or out-of-control. Output layer of network uses 0 and 1 to represent in-control and out-of-control decisions. The data of input patterns must be scaled first. Linear transformation is used to set the range of input values between [0, 1] to avoid extreme values from affecting network training results. Some parameters of the network model (learning rate, training number, errors, and number of hidden layer nodes) need to be carefully set to achieve good model performance. Uniformly distributed random numbers, which ranges between [-1, 1] are used to set interconnected weights and biased weight vectors for the training patterns of the model. Sigmoid function is used in the model and the numerical range is between [0, 1].

$$f(x) = \frac{1}{1+e^{-net_j}} \quad \ldots(4)$$

Standard energy function [Eq. (5)] is used to calculate variation between expected output and network output.

$$E = \frac{1}{2}\sum_j (T_j - O_j)^2 \quad \ldots(5)$$

where O_i is i-th set of wavelet characteristic of network output at defect determination and T_i is relative target of O_i. Stop criterion of proposed model is based on the proposition of Ivezi[22], who used Root Mean Square Error (RMSE) and early stopping technique to set the parameters.

Wavelet-based Hotelling Statistic Approach (WHS)

WHS approach decomposes an image of (*S* x *T*) pixels into a set of sub-images, each of which has a size of (*s* x *t*) pixels and is a multivariate processing unit. Original image has *u* x *v* (*S*/*s* x *T*/*t*) multivariate processing units, each of which can be further decomposed into *k* x *l* wavelet processing units. For each wavelet processing unit, wavelet transform can be applied to the region of (*s*/*k* x *t*/*l*) pixels to obtain FWCs through calculations. Multivariate statistic T^2 integrates multiple wavelet characteristics into a T^2 value for each multivariate processing unit. This T^2 value can be regarded as a distance value of a multivariate processing unit. The larger the T^2 statistic value, the more distinctive the region is from the normal area. Thus, more easily the region can be judged as defective.

Proposed wavelet based approach assumes that size of a multivariate processing unit is 4 x 4 (*s* x *t*) pixels and size of a wavelet processing unit is 2 x 2 (*k* x *l)* pixels. One multivariate processing unit will have 2 x 2 (*s*/*k* x *t*/*l*) wavelet processing units. That is, four wavelet processing units $W(x_k, y_l)$ can be defined as one multivariate processing unit $N(x, y)$, where *k* and *l* are integers and (1d"*k*, *l*d"2). Corresponding spatial coordinates of $W(x_k, y_l)$ are a square (size 2 x 2 pixels) from $g(4\times x+k, 4\times y+l)$ to $g(4\times x+k+1, 4\times y+l+1)$. Thus, one $N(x, y)$ includes four $W(x_k, y_l)$, which are $W(x_1, y_1)$, $W(x_1, y_2)$, $W(x_2, y_1)$ and $W(x_2, y_2)$. One $W(x_k, y_l)$ can be decomposed by wavelet transform to obtain one approximated characteristic $A(x_k, y_l)$ and three detail characteristics $D_1(x_k, y_l)$, $D_2(x_k, y_l)$ and $D_3(x_k, y_l)$.

Multivariate control charts are usually used for quality monitoring of processes with multiple related variables. Lowry & Montgomery[23] and Montgomery[24] introduced and compared procedures and functions of multivariate control charts in statistical process control (SPC). Hotelling's T^2 statistic[25] measures statistical distance of the observation from estimated mean of in-control data population while taking into account the estimated variance-covariance structure of in-control data population. The formulas of T^2 multivariate control procedure[24] can be rewritten as Eqs (6) to (15) to represent a multivariate process of images. Let $Y_{W(x_k, y_l), p}$ be *p*-th image characteristic of a wavelet processing unit $W(x_k, y_l)$, then $\overline{Y}_{N(x, y)}$ is mean matrix of image characteristics in a multivariate processing unit $N(x, y)$ and can be expressed as

$$\overline{Y}_{N(x, y)} = \left[\frac{1}{k\times l} \sum_{r=1}^{k} \sum_{s=1}^{l} Y_{W(x_r, y_s), p} \right]_{p\times 1} \quad \ldots(6)$$

$\overline{Y}_{N(r, s), p}$ is mean value of *p*-th image characteristic of $N(r, s)$. The sample mean matrix of image characteristics of an image is

$$\overline{\overline{Y}} = \left[\frac{1}{u\times v} \sum_{r=0}^{u-1} \sum_{s=0}^{v-1} \overline{Y}_{N(r, s), p} \right]_{p\times 1} \quad \ldots(7)$$

$S^2_{N(x, y), p}$ is variance of *p*-th image characteristic of $N(x, y)$ and $S_{N(x, y), p, q}$ is covariance of *p*-th and *q*-th image characteristics of $N(x, y)$. They can be written as

$$S^2_{N(x, y), p} = \frac{1}{k\times l-1} \sum_{r=1}^{k} \sum_{s=1}^{l} \left(Y_{W(x_r, y_s), p} - \overline{Y}_{N(x, y), p} \right)^2 \quad \ldots(8)$$

$$S_{N(x, y), p, q} = \frac{1}{k\times l-1} \sum_{r=1}^{k} \sum_{s=1}^{l} \left(Y_{W(x_r, y_s), p} - \overline{Y}_{N(x, y), p} \right) \left(Y_{W(x_r, y_s), q} - \overline{Y}_{N(x, y), q} \right) \quad \ldots(9)$$

Sample variance of *p*-th image characteristic and sample covariance of *p*-th and *q*-th image characteristics of an image are

$$S^2_p = \frac{1}{u\times v} \sum_{r=0}^{u-1} \sum_{s=0}^{v-1} S^2_{N(r, s), p} \quad \ldots(10)$$

$$S_{p, q} = \frac{1}{u\times v} \sum_{r=0}^{u-1} \sum_{s=0}^{v-1} S_{N(r, s), p, q} \quad \ldots(11)$$

Multivariate matrices used in this study can be expressed as

$$Y_{W(x_k, y_l)} = \begin{bmatrix} A(x_k, y_l) \\ D_1(x_k, y_l) \\ D_2(x_k, y_l) \\ D_3(x_k, y_l) \end{bmatrix}_{4\times 1}$$

$$\overline{Y}_{N(x, y)} = \begin{bmatrix} \overline{A}(x, y) \\ \overline{D}_1(x, y) \\ \overline{D}_2(x, y) \\ \overline{D}_3(x, y) \end{bmatrix}_{4\times 1} = \begin{bmatrix} \frac{1}{k\times l} \sum_{r=1}^{k} \sum_{s=1}^{l} A(x_r, y_s) \\ \frac{1}{k\times l} \sum_{r=1}^{k} \sum_{s=1}^{l} D1(x_r, y_s) \\ \frac{1}{k\times l} \sum_{r=1}^{k} \sum_{s=1}^{l} D2(x_r, y_s) \\ \frac{1}{k\times l} \sum_{r=1}^{k} \sum_{s=1}^{l} D3(x_r, y_s) \end{bmatrix}_{4\times 1} \quad \ldots(12)$$

Normal texture images are used to estimate parameters of standard texture characteristics. The sample mean matrix ($\overline{\overline{Y}}$) and sample covariance matrix (S) describe properties and relations between normal and defect images. $\overline{\overline{Y}}$ and S are defined as

$$\overline{\overline{Y}}=\begin{bmatrix}\overline{\overline{A}}\\ \overline{\overline{D}}_1\\ \overline{\overline{D}}_2\\ \overline{\overline{D}}_3\end{bmatrix}_{4\times 1}, \qquad S=\begin{bmatrix} S_A^2 & S_{A,D_1} & S_{A,D_2} & S_{A,D_3}\\ S_{D_1,A} & S_{D_1}^2 & S_{D_1,D_2} & S_{D_1,D_3}\\ S_{D_2,A} & S_{D_2,D_1} & S_{D_2}^2 & S_{D_2,D_3}\\ S_{D_3,A} & S_{D_3,D_1} & S_{D_3,D_2} & S_{D_3}^2\end{bmatrix}_{4\times 4} \qquad ...(13)$$

where S_p^2 is sample variance of p-th wavelet characteristic of an image, $S_{p,q}$ is sample covariance of p-th and q-th wavelet characteristics of an image.

T^2 statistic value of multivariate processing unit $N(x, y)$ of a testing image can be defined as

$$T^2_{N(x,y)} = k \times l\left[\overline{Y}_{N(x,y)} - \overline{\overline{Y}}\right]^T S^{-1}\left[\overline{Y}_{N(x,y)} - \overline{\overline{Y}}\right] \qquad ...(14)$$

where k x l is the number of wavelet process units in a multivariate processing unit. $\overline{Y}_{N(x,y)}$ is mean matrix of image characteristics in multivariate processing unit of a testing image. $\overline{\overline{Y}}$ and S are respectively mean matrix and covariance matrix of image characteristics of a normal image. The upper control limit (UCL) is as

$$\frac{p(s-1)(t-1)}{st-s-p+1} F_{\theta,p,(st-s-p+1)} \qquad ...(15)$$

where F is a tabulated value of F distribution at significance level of θ. Therefore, if a multivariate processing unit $N(x, y)$ of a testing image $f(x, y)$ has a higher value, it implies that the region contains defects in testing image. On the contrary, a lower T^2 value signifies that no defect exist in corresponding region of the image.

Experiments and Analyses

To evaluate performance of proposed approaches, experiments were conducted on real LED chips, provided by a LED chips manufacturing company in Taiwan. LED chip images (270), of which 90 have no defects and 180 have various water-drop defects, were tested. All samples were randomly selected from manufacturing process of LED chips. Cross-validation technique was applied to training process of WBPN approach. Samples were divided into three disjoint sets: one-half samples used as a training set for network learning; one quarter used as a validation set to tune the parameters of a network; and remaining quarter used as a test set to assess performance of a fully-trained network. All experiments were implemented on a Pentium IV personal computer with 2.6GHz CPU and 512 MB RAM, and all programming was done in C language.

To maximize number of LED chips on a wafer, every chip was located very close to its neighboring chips. As carrier plate moves to have the image of next chip captured, the movement might cause CCD to deviate from its original position and the image capturing device to vibrate. Thus, images of all chips might be captured with slight differences. That is, not all the chips are located in exactly same positions in their individual images. As a result, two areas are needed for each image to specify the locations of two different background textures, in which water-drop defects may possibly exist. LED emitting area (Fig. 3) and bonding pad (Fig. 4) need to be separated first and then individually apply proposed methods to detect defects.

Emitting area in the outer area of LED chip contains uniform texture. Since wavelet transform can process images of rectangular shapes, a specially made background must be added to convert different shape region into a rectangular one. Thus, gray levels of area falling outside the outer area were changed to average gray level of normal chip images (Fig. 3 b). With such a manipulated background, a rectangular region for wavelet transform was obtained and also affected non-emitting region was minimized. Once mixed image is transformed into wavelet domain, non-emitting region will not interfere in feature extraction of emitting region. Similarly, this procedure is also applied to defect detection on LED bonding pad except additionally taking median filtering operation. In central area of an LED chip is a bonding pad, which contains statistical texture with random particles like pepper noises. The more similar the gray levels of particles on bonding pad and water-drop defect, the more difficult is to distinguish defect and random particles. Median filter[26] was used to smooth particles on random texture. Mask (size 11 x 11 pixels) is capable of smoothing all random particles in

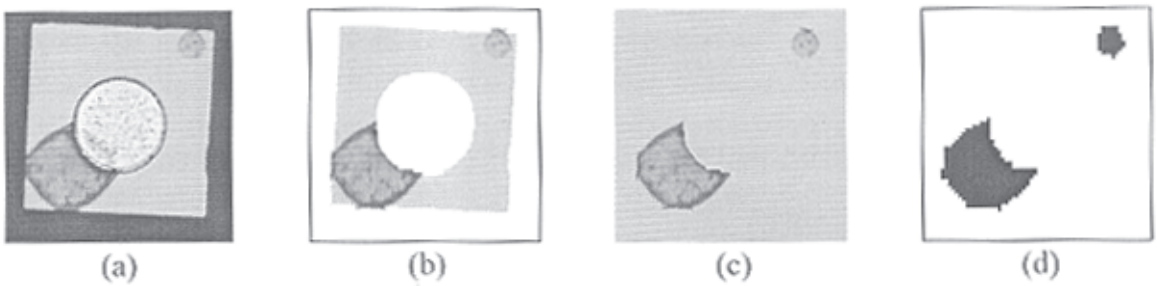

Fig. 3—Procedure of detecting defects on LED emitting area: a) Input an LED chip image; b) Separate outer area of LED chip; c) Change gray levels of area falling outside outer area; d) Apply proposed method to detect defects

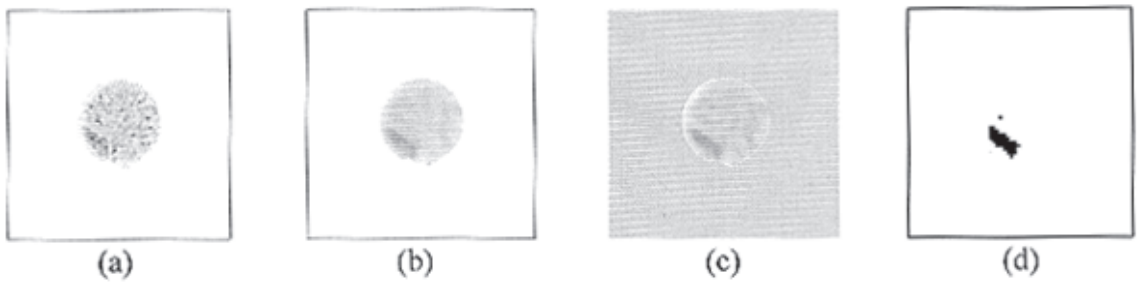

Fig. 4—Procedure of detecting defects on LED bonding pad: a) Separate central area of LED chip; b) Take median filtering on central area; c) Change gray levels of area falling outside central area; d) Apply proposed method to detect defects

testing samples (Fig. 4 b). Then, filtered images were conducted for gray level changes of the area falling outside central area for the same purpose described in Fig. 3 b.

For precisely presenting locations of water-drop defects, most appropriate size of a wavelet processing unit was found to be 2 x 2 pixels in wavelet transformation. Input patterns of WBPN model, each including FWCs, were obtained from 16,384 sets of a testing image. Testing results of WBPN models can be affected by parameter settings, number of training samples, input patterns of network, and so on. Early stopping technique was adopted for preventing overfitting and improving generalization. Training set was used for computing gradient and updating network weights and biases. Error on validation set was monitored during training process. Validation error normally decreases during initial phase of training, so does the training set error. However, when network begins to overfit the data, validation error typically begins to rise. When validation error increases for a specified number of iterations, training is stopped, and weights and biases at the minimum validation error are returned. The test set error is used to compare different network models.

After conducting various experiments, best parameter settings of WBPN model found for water-drop defect detection of bounding area and emitting area were, respectively: i) number of hidden layers, 1, 1; ii) number of hidden layer nodes, 6, 3; iii) learning rate, 0.5, 1.0; iv) momentum, 0.5, 0.5; and v) iteration cycles, 38, 9. Index RMSE is used to evaluate performance of network models. RMSE indices of two WBPN models with the given parameter settings are 0.056 and 0.068 for bounding area and emitting area, respectively.

For proposed WHS approach, most appropriate size of a multivariate processing unit was found to be 4 x 4 pixels after conducting various experiments. At this size, this method achieves best performance considering sample training time, recognition time of testing period, size of defect area and other factors in multivariate processing.

To verify performance of proposed methods, results of detecting water-drop defects by Otsu method[27], Mahalanobis distance (MD) method[5], proposed WBPN and WHS approaches were compared against those provided by professional inspectors (Fig. 5). MD, WBPN and WHS methods were found to detect most of the water-drop defects while Otsu method misses some defect regions. Higher the performance evaluation indices [$(1-\alpha)$, $(1-\beta)$], more accurate the detection results. Statistical type I error α suggests the probability of producing false alarms, i.e. detecting normal regions as defects. Statistical type II error β implies the probability of producing missing alarms, which fail to alarm real defects. Area of normal region detected as defects was

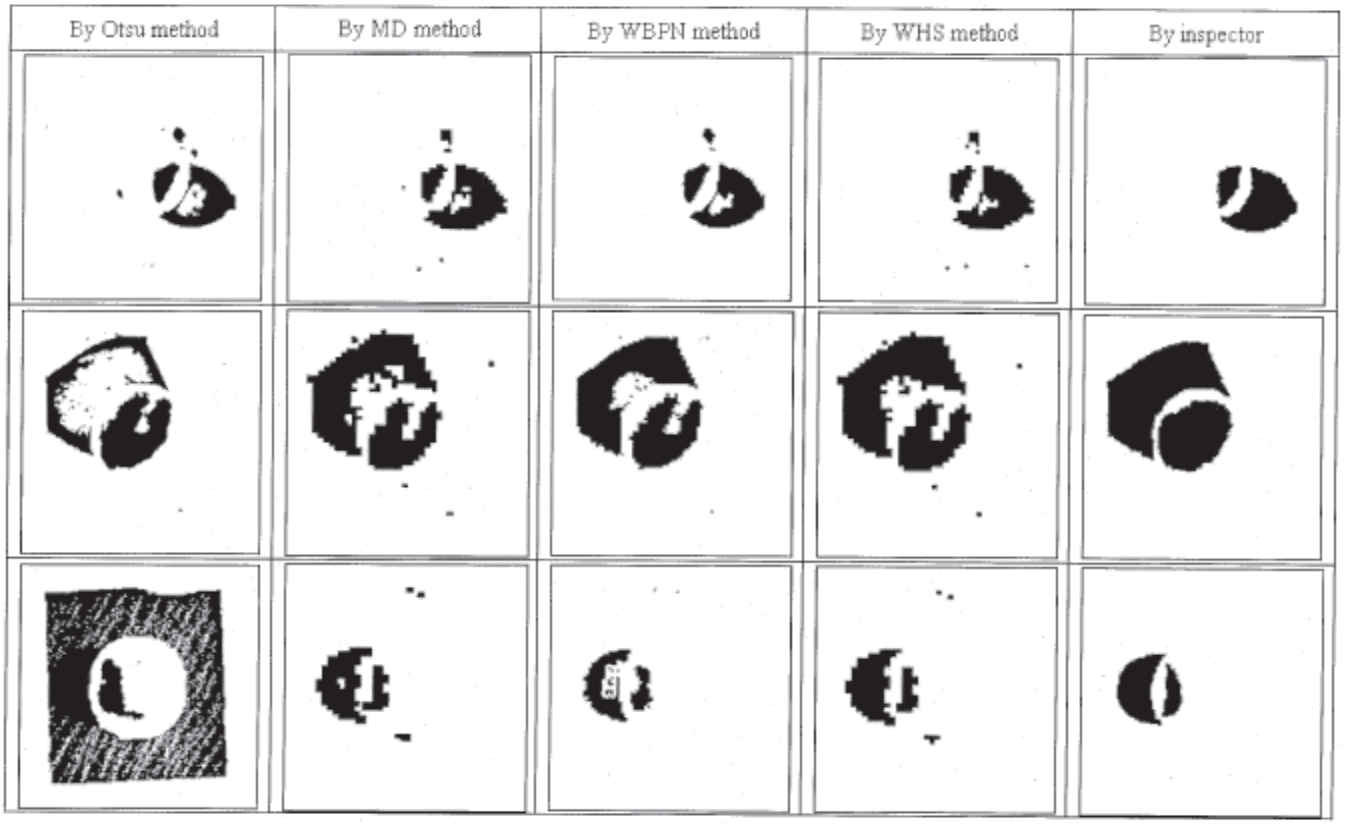

Fig. 5—Partial detection results of Otsu, MD, WBPN, and WHS methods and professional inspector

divided by the area of actual normal region to obtain type I error, and the area of undetected defects by the area of actual defects to obtain type II error. Correct classification rate (CR) is defined as

$$CR = (N_{cc} + N_{dd}) / N_{total} \times 100\% \quad \ldots (16)$$

where N_{cc} is pixel number of normal textures detected as normal areas, N_{dd} is pixel number of ripple defects detected as defective regions, and N_{total} is total pixel number of a testing image.

Average detection rates *(1-β)* of all testing samples were: Otsu method, 86.6; MD method, 88.5; WBPN method, 90.8; and WHS method, 92.4% (Table 1). Proposed wavelet based neural network and multivariate statistical approaches have higher detection rates *(1-β)* and CRs than do the two traditional methods applied to LED chip images. WBPN and WHS methods excel in their ability of correctly discriminating water-drop defects from normal regions.

Average processing time (APT) for an image of 256 x 256 pixels is as follows: Otsu method, 1.84; MD method, 2.75; WBPN method, 2.26; and WHS method, 2.32 seconds. Proposed two methods have shorter APT than MD method. APT of WHS method is very close to that of WBPN method. However, in training stage, WHS method takes less than 1 second to calculate related multivariate parameters when a suitable image is selected in advance. On the contrary, training process of WBPN method is very time-consuming (1.4-1.6 min).

As decision threshold value changes[28], so does its false alarm rate (□) and detection rate (1-β). When various decision thresholds [Eq. (15)] are used, their pairs of □ and (1-β) are plotted as points on a Receiver Operating Characteristic (ROC) curve. More the ROC plot approaches the upper-left corner (Fig. 6), the better the test performs; upper-left corners (Fig. 6) are optimum points (1-β, 100%; □, 0%). In industrial practices, (1-β) > 90% and □ < 10% are a good rule of thumb for performance evaluation of a vision system. Accordingly, proposed WHS and WBPN approaches, with their ROC plots closer to the upper-left corner, outperform two traditional methods.

Table 1—Performance indices of all testing samples by the four methods

	Otsu method	MD method	WBPN method	WHS method
α, %	9.0	6.9	4.4	6.1
(1-ß), %	86.6	88.5	90.8	92.4
CR, %	89.7	92.8	96.9	95.6
Time, s	1.84	2.75	2.26	2.32

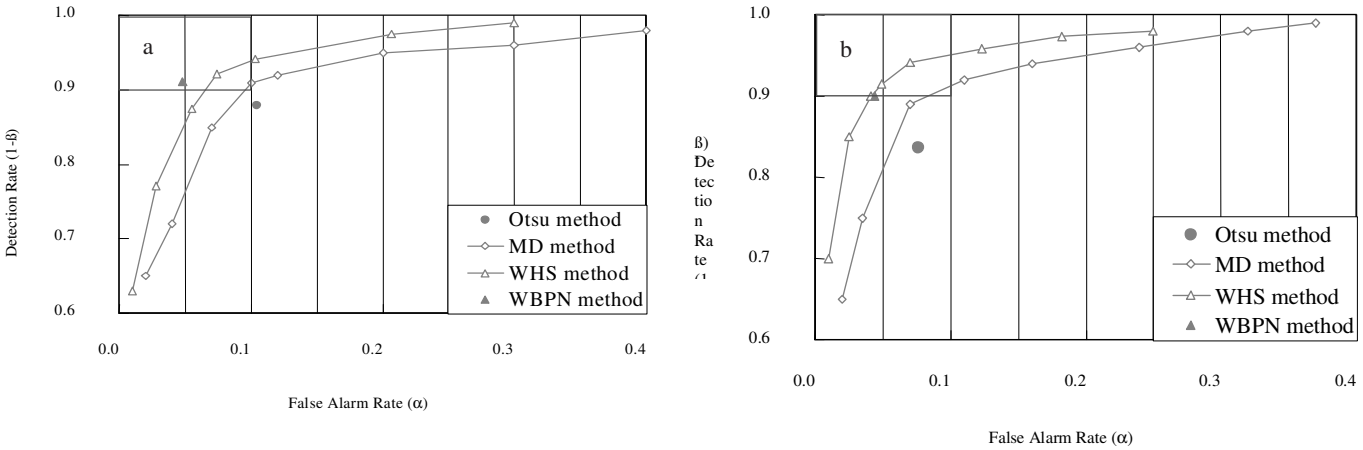

Fig. 6—ROC plots of Otsu, MD, WBPN, and WHS methods for: a) Bonding pad; b) Emitting area

WHS method has higher defect detection rate and WBPN method has lower . When major concern of detection is on the area of erroneously detected defects, WBPN method is the best choice because it has lowest . On the other hand, if the focus is on accurate areas of detected defects, WHS method should be applied because of its higher accuracy in detecting real defect areas.

Performance of proposed methods can be limited by normal distribution assumptions, lighting changes, and background properties. In proposed WHS method, if Y_i does not follow a multivariate normal distribution, the pre-defined UCL values [Eq. (15)] cannot be used to determine whether transformed value of statistic T^2 is large enough for an out-of-control signal. For defect detection, multiple measures of image characteristics are represented by multiple random variables. Typically, probability plotting is used to determine whether sample data conform to normal distributions[29]. In present experiments, normal probability plots of FWCs constructed from distributions $Y_1 \sim Y_4$ all approximate straight lines, indicating that the multivariate data are normally distributed.

In addition, since computation of multivariate statistics is based on mean vector and covariance matrix of training samples, lighting changes may lead to an increase of variation in statistics and result in a decline of defect detection performance. Thus, it is recommended to re-compute mean vector and covariance of training samples whenever illumination is significantly changed. Also, proposed method is not recommended for detecting defects embedded in structural textures because it is designed to identify defects in random textures.

Concluding Remarks

Wavelet-based back-propagation network and multivariate statistical approaches use back-propagation network algorithm and multivariate T^2 test to judge the existence of water-drop defects through multivariate

processes of combining image characteristics from wavelet decomposition of local image blocks. Experimental results show that the WBPN and WHS approaches respectively achieve detection rates of above 90.8% and 92.4%, and false alarm rates of below 4.4% and 6.1% in detecting water-drop blemishes across two different background textures. As indicated in the ROC curve analysis, WBPN and WHS approaches have lower false alarm rates and better detection rates than do Otsu and MD methods. This research contributes a solution to a common surface defect detection problem of LED chips and offers a computer-aided visual defect inspection system to meet the inspection and quality control request.

References

1 Lin C S, Ho C W, Wu C Y, Miau L H & Lin L, Automatic inspection device for HCV antibody rapid test strips for the production line, *J Sci Ind Res*, **63** (2004) 251-258.

2 Malamas E N, Petrakis E G M, Zervakis M, Petit L & Legat J D, A survey on industrial vision systems, applications and tools, *Image & Vision Computing*, **21** (2003) 171-188.

3 Huang C J, Clustered defect detection of high quality chips using self-supervised multilayer perceptron, *Expert Syst with Applications*, **33** (2007) 996-1003.

4 Siew L H, Hodgson R M & Wee L K, Texture measures for carpet wear assessment, *IEEE Trans Pattern Analysis & Machine Intelligence*, **10** (1988) 92-150.

5 Latif-Amet A, Ertüzün A & Ercil A, An efficient method for texture defect detection: sub-band domain co-occurrence matrices, *Image & Vision Computing*, **18** (2000) 543-553.

6 Chan C H & Pang G K H, Fabric defect detection by Fourier analysis, *IEEE Trans Ind Applications*, **36** (2000) 1267-1276.

7 Kumar A & Pang G K H, Defect detection in textured materials using Gabor filters, *IEEE Trans Ind Applications*, **38** (2002) 425-440.

8 Lin H D & Ho D C. Detection of tiny surface defects using DCT based enhancement approach in computer vision systems, *IEEE/ASME Int Conf Advanced Intelligent Mechatronics (IEEE/ASME AIM)* 2005, 373-378.

9 Lin H D & Chiu S W, Computer-aided vision system for MURA-type defect inspection in liquid crystal displays, *Lecture Notes in Compu Sci*, **4319** (2006) 442-452.

10 Lu C J & Tsai D M, Defect inspection of patterned TFT-LCD panels using a fast sub-image based SVD, *Int J Prod Res*, **42** (2004) 4331-4351.

11 Maruo K, Shibata T, Yamaguchi T, Ichikawa M & Ohmi T, Automatic defect pattern detection on LSI wafers using image-processing techniques, *IEICE Trans Electron*, **E82** (1999) 1003-1012.

12 Shankar N G & Zhong Z W, Defect detection on semiconductor wafer surfaces, *Microelectronic Engg*, **77** (2005) 337-346.

13 Shankar N G & Zhong Z W, A rule-based computing approach for the segmentation of semiconductor defects, *Microelectronics J*, **37** (2006) 500-509.

14 Fadzil M H A & Weng C J, LED cosmetic flaw vision inspection system, *Pattern Analysis & Application*, **1** (1998) 62-70.

15 Gonzalez R C & Woods R E, *Digital Image Processing*, **2nd edn** (Prentice-Hall, Upper Saddle River, NJ) 2002, 349-403.

16 Arivazhagan S & Ganesan L, Texture segmentation using wavelet transform, *Pattern Recognition Lett*, **24** (2003) 3197-3203.

17 Bashar M K, Matsumoto T & Ohnishi N, Wavelet transform-based locally orderless images for texture segmentation, *Pattern Recognition Lett*, **24** (2003) 2633-2650.

18 Kameyama K, Kosugi Y, Okahashi T & Izumita M, Automatic defect classification in visual inspection of semiconductors using neural networks, *IEICE Trans Inform & Syst*, **E81** (1998) 1261-1271.

19 Kang B S & Park S C, Integrated machine learning approaches for complementing statistical process control procedures, *Decision Support Syst*, **29** (2000) 59-72.

20 Chen F L & Liu S F, A neural-network approach to recognize defect spatial pattern in semiconductor fabrication, *IEEE Trans Semiconductor Manuf*, **13** (2000) 366-373.

21 Kumar A, Neural network based detection of local textile defects, *Pattern Recognition*, **36** (2003) 1645-1659.

22 Ivezi23 D, Short-Term Natural Gas Consumption Forecast, *FME Trans*, **34** (2006) 165-169.

23 Lowry C A & Montgomery D C, A review of multivariate control charts, *IIE Trans*, **27** (1995) 800-810.

24 Montgomery D C, *Introduction to Statistical Quality Control*, **5th edn** (John Wiley & Sons, Hoboken, NJ) 2005, 491-504.

25 Hotelling H, Multivariate quality control, in *Techniques of Statistical Analysis*, edited by C Eisenhart *et al* (McGraw-Hill, New York, NY) 1947, 111-184.

26 Jain R, Kasturi R & Schunck B G, *Machine Vision*, **Int edn** (McGRAW-Hill, New York, NY) 1995, 80-83.

27 Otsu N, A threshold selection method from gray-level histogram, *IEEE Trans Syst, Man, Cybernetics*, **9** (1979) 62-66.

28 Montgomery D C & Runger G C, *Applied Statistics and Probability for Engineers*, **2nd edn** (John Wiley & Sons, New York, NY) 1999, 296-304.

29 Hair J F, Anderson R E, Tatham R L & Black W C, *Multivariate Data Analysis*, **5th edn** (Prentice-Hall, Upper Saddle River, NJ) 1998, 70-73.